**THE EUROPEAN
PHYSICAL JOURNAL D**

A spectroscopical study of H₂ emission in a simply magnetized toroidal plasma

R. Barni[1], P. Alex[1], E. Ghorbanpour[2], and C. Riccardi[1,a]

[1] Dipartimento di Fisica G.Occhialini, Università degli Studi di Milano-Bicocca, Piazza delle Scienza 3, I-20126 Milano, Italy
[2] Department of Physics, Faculty of Science, University of Guilan, P.O. Box 41335-1914, Rasht, Iran

Abstract. A noninvasive diagnostic technique relying on optical emission spectroscopy is used for studying plasma confined in a purely toroidal magnetic field. Visible emission lines of molecular hydrogen were specifically targeted. Bi-dimensional structures and poloidal plasma profiles were reconstructed from the emissivity distribution of hydrogen Fulcher system using a tomographic method. A few details concerning the methods employed to capture different emission viewlines, data reduction and tomographic reconstruction techniques are also addressed. We report also the first measurement of the excitation temperature of the H₂ [3c] level in the center of the plasma column, $T_{\mathrm{exc}} = 0.67 \pm 0.11$ eV.

1 Introduction

The quest for finding new sources of energy has generated large interest in magnetized plasmas where plasma is confined in toroidal device such as tokamaks and stellarators aiming to produce energy through controlled thermonuclear fusion [1,2]. In particular, there is an ongoing effort aimed to better understand the effect of anomalous particle transport in reducing the confinement in magnetized plasma [3]. This phenomenon is quite general and related to the dynamical effects due to turbulence, which arise naturally in magnetized plasmas [4]. In particular, there is evidence of drift-wave turbulence in magnetically confined plasmas and, associated to that, the appearance and build-up of large amplitude density fluctuations in the edge region of plasmas, strongly contributing to turbulent cross-field particle and energy fluxes [4]. The turbulence measurements are generally more complicated in plasmas than in fluids due to the faster time scales and to the difficulties in measuring locally microscopic parameters such as the plasma density and temperature [5]. Another approach is related to the use of the electromagnetic radiation emitted by the plasma state. This usually escapes from the plasma and could be collected from outside, without a direct disturbance of the system. As a tool for the study of plasma turbulence, optical diagnostics could be demanding too [6]. Since in plasma turbulence the associated autocorrelation times are in the range of a few microseconds to tens of microseconds, the diagnostics should be faster than these time scales. Optical emission spectroscopy (OES) is usually fast enough. For instance, in a hydrogen plasma, the lifetime of hydrogen $n = 3$ state, emitting the H_α line, is about 10 ns. However, even in a simple hydrogen low-temperature plasma, OES reveals many features arising from the complex plasma gas phase. Although atomic hydrogen dominates emission, it is common to spot emission also from the rich structure of excited levels of the H₂ molecules [7]. Such features in the emission spectra are suitable to study particular phenomena happening in the plasma, be it those arising due to presence of minority ions, the recombination or the dynamical effects induced by the collisions with neutrals [8]. The continuous improvement in radiative collisional models also opens up the concrete possibility to relate spectroscopical data to constrain or even to measure more fundamental plasma parameters [9,10]. Here, we present the application of an OES passive optical diagnostics to the study of emissivity in a simply magnetized toroidal (SMT) device using a low-resolution visible spectrometer. In particular, our aim will be to reconstruct the 2D pattern of emissivity of H₂ molecular states of the so-called Fulcher-α band system, the $2p\pi^3\Pi_u[3c] \rightarrow 2s\sigma^3\Sigma_g^+[2a]$ transitions [11].

2 Experimental setup

Schematic of the experimental setup is shown in Fig. 1. The Thorello device consists of four 75° curved and corrugated stainless steel sectors. Each of these four sectors is joined together by four junctions, each with an angular opening of 15°, and is provided with ports

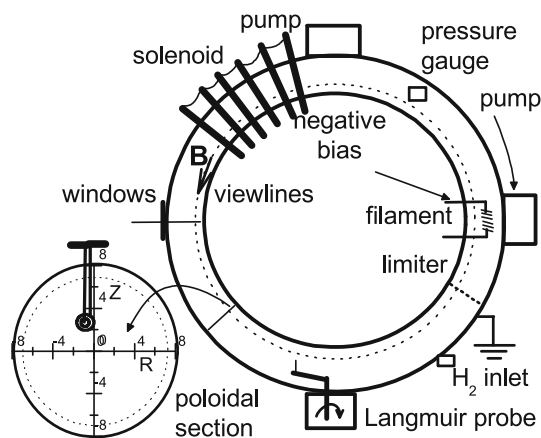ᵃ e-mail: claudia.riccardi@unimib.it (corresponding author)

Fig. 1 Layout of the Thorello device with diagnostics ports

Fig. 2 The view-line set implemented in the Thorello device and their covering of the poloidal cross-section mesh cells

for pumping, diagnostics and plasma source. All joined together they form a complete torus with a major radius of 40 cm and a minor radius of 8.75 cm. Each sector is garlanded by 14 evenly spaced circular coils, 56 altogether, which are fed in series with a DC current provided by an Eutron TVR-112 stabilized supply, with rating of 575 A and 150 V, capable of 85 kW power. Each of these coils consists of 12 copper winding pipes with square cross section and circular hole for water cooling. This arrangement forms the toroidal field coils for the device capable of applying a maximum purely toroidal field of 0.2 T (SMT configuration). In addition to the toroidal field, two vertical ring coils in Helmholtz arrangement, each with major and minor radii of 80 cm and 2 cm, respectively, are held horizontally 20 cm above and below the equatorial plane of the device. These two coils produce a mostly vertical field which adds to the purely toroidal field, which could be used to trim the properties and spatial distribution of the plasma state [12]. Base pressure of less than $1 \cdot 10^{-4}$ Pa is achieved in the system using a couple of turbo-molecular pumps backed by two rotary pumps. Experiments were normally performed by filling high purity hydrogen gas up to a pressure of a few 10^{-2} Pa. Plasma is produced by thermionic emission of three intertwined thoriated tungsten filaments bent in a 13 turns spiral shape (diameter 7 mm and length of 3 cm), placed with the axis aligned to the magnetic field about the center of the poloidal cross section. The filament is supported by using water cooled copper tubes. The filament is heated by passing a current of tens of ampere and discharge is struck between the hot filament (cathode) and the grounded vacuum vessel (anode) by applying a potential difference of about 150 V. More precisely a limiter, a hollow disk of 15 cm diameter, short-circuits the vertical electric field. The plasma produced in the chamber has almost complete toroidal uniformity with sharp gradients toward the vessel wall. Typical plasma parameters estimated using Langmuir probes at the radial center of the device are given by $T_e \sim 4$ eV, $T_i \sim 0.2$ eV, $N_e \sim 10^{11}$ cm^{-3} [13,14].
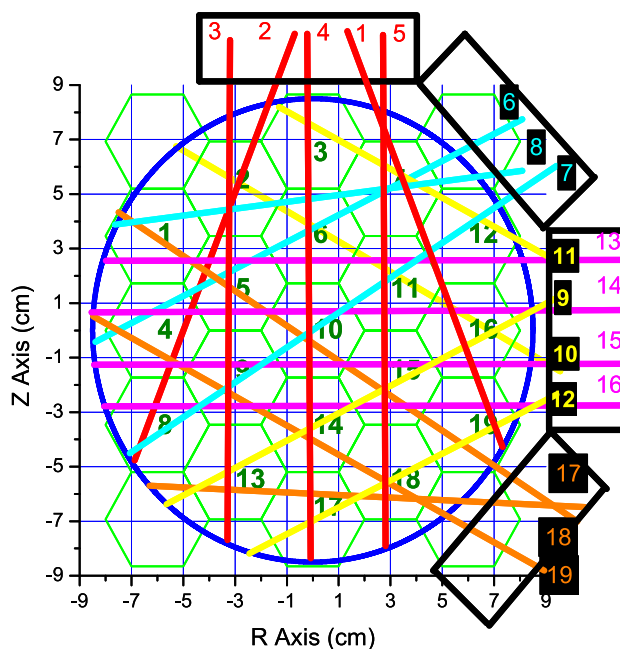
The plasma produced is confined by the applied toroidal field and substantially uniform along the magnetic field lines. So its dynamics is happening basically in the poloidal cross section [14]. Such plasma states are normally turbulent in nature, showing high level of fluctuations with rms up to 50% of their mean value. The arrangement helps in maintaining a steady-state plasma in DC mode for up to few hours without significant changes in mean plasma parameters. Althought the lack of a rotational transform implies that a magnetohydrodynamic equilibrium does not exist in the system, the improvement in the confinement time achieved by the poloidal limiter and the steady-state plasma conditions enable the device as a typical test bed for OES.

3 OES diagnostics

In order to demonstrate the capabilities of the proposed diagnostics, we have performed a few measurement in our magnetized plasma device. We take advantage of the steady-state stable conditions of the SMT plasma. The light emitted from the plasma could be collected from the windows placed in the sector junction opposite to the filament location (see Fig. 1), from which the full poloidal cross section can be viewed [7]. A set of 19 viewlines was implemented, with structures fitting to the window shape, allowing to collect light with an optical fiber in an easy but reproducible way (see Fig. 2). Each viewline contains actually the emission from a truncated conical volume of the plasma, with a base radius of at most, even for the longest viewlines, 5 mm. Because the whole set of viewlines can-

not be viewed simultaneously, we aimed to measure the mean plasma emission spectra, averaging effects due to its fluctuations, induced by the turbulent state of the SMT plasmas. However, we wanted to extract information about the main contribution involved in the emissivity pattern, at least in the visible optical range.

Measurements of resolved mean spectra are obtained with a wide band, low-resolution spectrometer. The spectrometer (PS2000 by Ocean Optics) has a resolution of about 0.3 nm and a spectral band extending from 180 to 860 nm. It is equipped with a 10-μm slit, a holographic grating (600 lines/mm, blazed at 400 nm) and a coated quartz lens to increase sensitivity in UV [15]. A 800-μm, UV-enhanced optical fiber from Avantes was used to bring the light collected from the viewlines to the spectrometer. Viewlines spectra can be analyzed separatedly, but the whole dataset allows to reconstruct a 2D map of the plasma average emissivity, covering the poloidal cross section with a rough mesh of hexagonal cells with a resolution of about 3.5 cm [7]. To reduce statistical uncertainty, we measure three times the full set of 19 viewlines, each set with a different random order, to mitigate effects due to plasma fluctuations as well as plasma parameters drift. Spectrometer acquisition times, in the order of hundreds milliseconds, were optimized to each viewline in order to accumulate a number of counts near to 4096, the limit of the spectrometer digitizer. All the spectra were cleaned by subtracting the relevant dark spectra [7]. The average intensity of each viewline was then evaluated, together with a statistical error. We also wish to point out that such acquisition times are much longer than the typical scale of fluctuations due to the turbulence in our plasmas. So each viewline spectrum records the average emission from the plasma column and a time resolved measure of the emissivity fluctuations requires much faster detectors.

4 Experimental results

The discharge OES spectra we are discussing about were taken from plasma driven by a 70-A filament current and a 150 V cathode bias, with a magnetic field of 70 mT, starting from a 0.1 Pa pure hydrogen gas. A typical spectrum measured is shown in Fig. 3. In the typical conditions of density and temperature of our plasma even for the most intense emission lines, the plasma column remains optically thin [7,14]. This could be also assessed by comparing the line shape measured from different viewlines, in particular those intersecting only the outer plasma regions. Apart from the more prominent Balmer lines, it is possible to spot several lines emitted from excited states of the hydrogen molecule. Among them the most suitable, because of their relative higher intensity and proximity to Balmer lines, given the limited resolution spectrometer, are a series of lines above 600 nm, near the H_α line and another group of
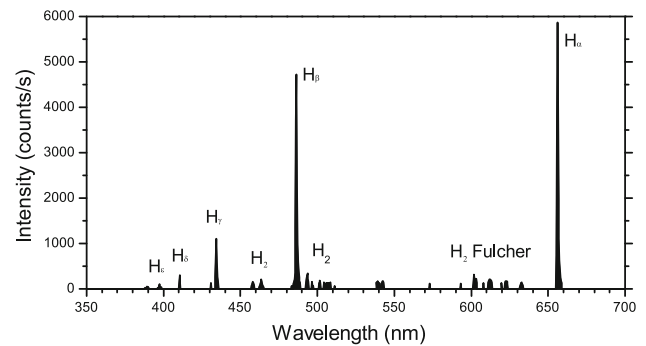

Fig. 3 A typical spectrum collected from a viewline of the Thorello plasma

lines at 458/463/493 nm near the H_β [11]. Then, it is possible to investigate both triplet and singlet states of hydrogen molecules. It should be noted, however, that in close parallel to hydrogen Lyman vs Balmer series, the observation of transitions from low-lying states to the ground state of hydrogen molecule requires the use of vacuum UV spectrometers and direct access, to circumvent windows absorption. OES is indeed limited to detect states with somewhat a high energy respect to the ground state, far greater than the typical mean electron energies. So the information refers mostly to the high energy tail of the electron population. In particular, we will discuss, in the rest of the paper, the lines corresponding to the Fulcher-α diagonal bands. They are usually the more bright ones in that region, at 602.0, 612.3, 622.6 and 632.9 nm. They are identified as the Q-band transitions between corresponding vibrational levels [(n,n)-Q1 with $n = 0 \ldots 3$], emitted from the de-excitation of subsequent excited vibrational levels of the [3c]-state of the hydrogen molecule [11].

As we have already discussed, we extracted a set of 19 viewline intensities for each of the selected lines, as well as of H_α for comparison, reported in Table 1. As it could be grasped from the data, the ratios between the intensities of the H_α and the H_2 633 nm line with the 602 one varied significantly along the different viewlines, well above the experimental uncertainties. This proves the presence of substantial spatial variations of the emissivity ratios, which could be traced to differences in the relative population of the excited states. These are due to spatial differences in the energies of the exciting agents. So this kind of experimental information could be used to gain insight into more fundamental plasma parameters. For instance the ratio of the intensity of the H_2 602 nm line with that of the H_α line varied between 5%, for the most intense viewline passing through the plasma column center, to less than 1% for peripheral viewlines looking the edges of the plasma. This implies that excitation of molecular hydrogen state is much reduced there. A collisional radiative model is needed to translate this kind of informations into quantitative estimates of plasma parameters.

Table 1 Mean intensities of emission lines from the different viewlines

View	H_α	602 nm	612 nm	623 nm	633 nm
1	834.7	22.3	14.6	11.8	8.26
2	1014.4	12.2	8.63	8.97	6.44
3	2207.8	51.7	32.8	29.3	22.3
4	2893.1	151.7	91.6	74.2	50.8
5	1488.0	50.6	30.0	27.2	19.1
6	2480.0	130.5	89.2	77.7	56.6
7	2383.2	97.5	70.2	64.6	44.5
8	1183.4	32.6	31.1	30.5	22.2
9	1427.8	25.1	16.4	14.6	10.5
10	686.7	6.17	3.52	2.65	2.48
11	502.5	13.3	7.84	5.62	3.93
12	2177.6	106.7	71.9	57.1	39.8
13	2518.5	141.8	90.3	72.7	52.4
14	2106.5	95.8	58.5	48.0	33.4
15	2012.5	54.4	36.6	31.2	21.5
16	2489.0	61.9	40.0	35.2	26.3
17	868.7	11.4	7.36	6.26	5.38
18	2226.1	73.8	56.0	53.2	37.4
19	1606.4	25.7	17.2	15.5	11.6

5 Data analysis and conclusions

The reconstruction of the 2D pattern of emissivity in the SMT poloidal cross section is then undertaken from the 19 viewline average datasets, as we have discussed in our previous works [7]. An OES tomography analysis was conducted by considering the poloidal circular cross section of the device, having 175 mm diameter, covered with 19 hexagonal mesh, each with side length of 20 mm. Though the resolution can be increased with more hexagons, by reducing the side length, this particular size has been chosen so to match the number of line of sight. The hexagonal geometry was chosen compared to the typical squared one, because it allows to cover almost the entire plasma cross section with minimum uncovered regions. Choice of different shapes for mesh tile and use of 2D decomposition using Chebyshev polynomial can be used when the number of viewlines available is more in number compared to the cell numbers [16]. Using the proposed mesh, each viewline covers an average of 4.2 hexagons and each cell is imaged by an average of 4 viewlines, as it could be grasped from Fig. 2. The measured intensity of light emitted along the nth viewline, I_n can be decomposed as a linear combination of the emissivity by an unit plasma volume, assumed to be constant in each of the crossed hexagons. Thus, it is given by $I_n = \Sigma_{m=1}^{19} W_{nm} \times J_m$, where W_{nm} is a matrix with nonzero entries that corresponds to the cells viewed by each viewline. In Figs. 4 and 5, we report the results for the first of the Fulcher-α diagonal band lines, compared with the Balmer H_α. Even with the limited resolution implied by relative small number of viewlines and so grid positions, the differences are clearly visible. Both emissivity patterns are peaking at the location of the filament magnetic shadow (cell 6 in Fig. 2). However, H_α emissivity shows
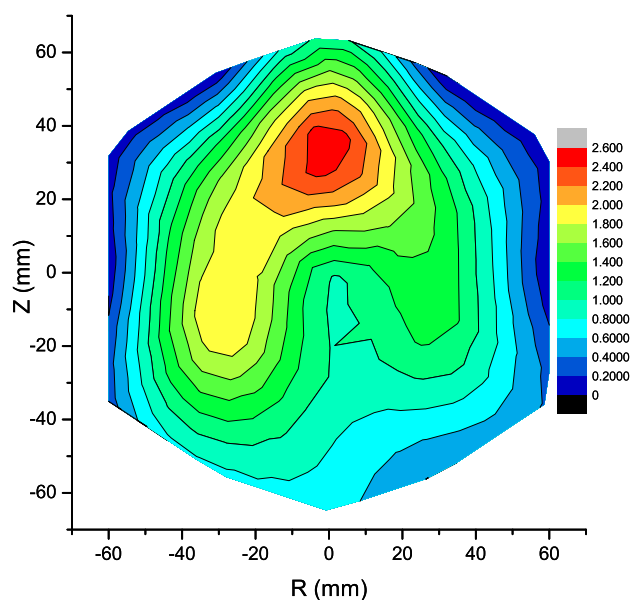

Fig. 4 Emissivity profile of the poloidal cross section for the H_α Balmer line

two pronounced tails extending downward to the edges, showing a strong asymmetry of the profile. The Fulcher-α (0-0) emission, however, is much more concentrated around the peak with a more symmetrical profile. So, it could be noticed that, contrary to naive expectations, the molecular line pattern is more concentrated in the central region, around the filament magnetic shadow in the poloidal cross-section respect to the Balmer line. Here, one could expect a depletion due to the higher dissociation of the hydrogen molecules there.

The analysis could be repeated for the other lines of the diagonal band, whose emissivity profiles are similar
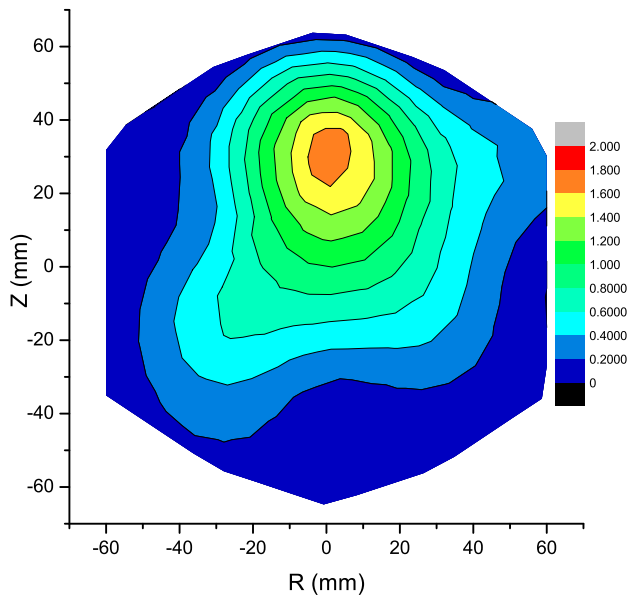
Fig. 5 Emissivity profile of the poloidal cross section for the H_2 Fulcher 602 nm line

Fig. 6 Measure of the excitation temperature of the H2 3c state in the cell corresponding to the brighter spot of the plasma column

to those already reconstructed for the (0,0) 602 nm line in Fig. 5, with some small differences. As an example of the potentiality of the OES diagnostics, in this preliminary report we analyze the information that could be extracted by comparing these profiles. Indeed, from the reconstructed intensities of the diagonal band, using the relevant lifetimes and branching ratios [17], it is possible to estimate the relative population of the first four vibrational levels of the excited H_2 [3c] state. This was applied to the data reconstructed for the central peak of the emissivity profiles (cell 6 in Fig. 2). As it could be seen from the semi-log plot of Fig. 6, their distribution is roughly that prescribed by the Boltzmann factor, from which it is possible to extract an effective excitation temperature or, as it sometimes referred to, a vibrational temperature of the excited state. After a simple linear regression, we estimate in this case a $T_{exc} = 0.67 \pm 0.11$ eV [18]. To put this number in perspective, one could notice that, in the reported experimental conditions, we have measured an average central electron temperature of 4.4 eV. On the other hand, such excitation temperature is clearly much higher than the gas temperature and possibly also than the ion one (which, however, was not measured in the present conditions). Slightly smaller but similar values of the excitation temperatures (in $0.45 - -0.70$ eV range) were evaluated in the center surrounding cells, while in the external cells the errors introduced by the tomographic inversion generally affect the precision of the emissivity estimate, preventing a meaningful evaluation of the temperatures.

As a conclusion, we would like to underline the capability shown by OES spectroscopical diagnostics to obtain spatially resolved distributions of emissivity and therefore population of excited states in the plasma gas phase. Thi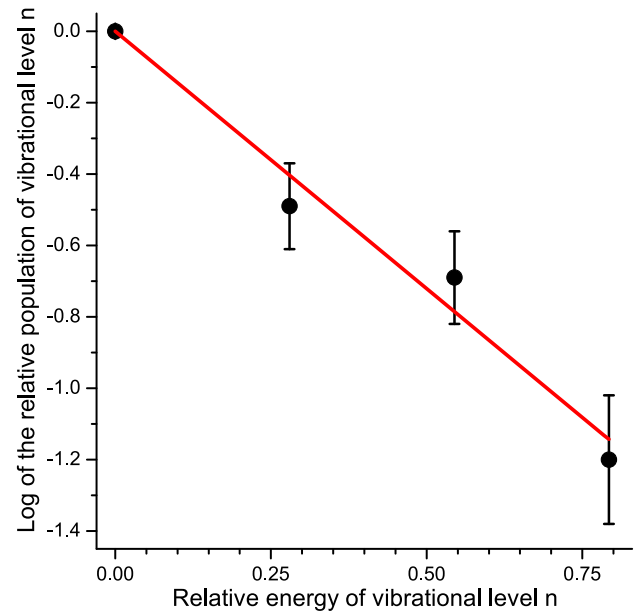s kind of experimental information has the potential to gain insight also into more fundamental plasma parameters, provided that the excitation mechanism could be underpinned. Data extracted from spectroscopy could also be used to test collisional radiative models and also more general simulations of the plasma state.

Author contributions

All the authors were involved in the preparation of the manuscript. All the authors have read and approved the final manuscript. We are also pleased to thank our technical staff at the PlasmaPrometeo Center for the support.

Data Availability Statement This manuscript has no associated data or the data will not be deposited. [Authors' comment: However raw data of the experiments will be made available upon request to the authors.]

References

1. L. Garzotti, C. Challis, R. Dumont et al., Nucl. Fusion **59**, 076037 (2019)
2. T. Klinger, T. Andreeva, S. Bozhenkov et al., Nucl. Fusion **59**, 112004 (2019)
3. F. Wagner, Plas. Phys. Control. Fusion **49**, B1 (2007)
4. G.R. Tynan, A. Fujisawa, G. McKee, Plas. Phys. Control. Fusion **51**, 113001 (2009)
5. T. Dudok de Wit, O. Alexandrova, I. Furno, L. Sorriso-Valvo, G. Zimbardo, Space Sci. Rev. **178**, 665 (2013)
6. A.J.H. Donné, Plas. Phys. Control. Fusion **48**, B483 (2006)
7. R. Barni, S. Caldirola, L. Fattorini, C. Riccardi, Plas. Sci. Tech. **20**, 025102 (2018)
8. T. Pierre, A. Escarguel, D. Guyormarc'h, R. Barni, C. Riccardi, Phys. Rev. Lett. **92**, 065004 (2004)
9. D. Wunderlich, S. Dietrich, U. Fantz, J. Quantitative Spectr. Radiative Trans. **110**, 62 (2009)
10. M. Capitelli, G. Colonna, L.D. Pietanza, G. D'Ammando, Spectr. Acta B **83–84**, 1 (2013)
11. A. Aguilar, J.M. Ajello, R.S. Mangina, G.K. James, H. Abgrall, E. Roueff, Astrophys. J. Suppl. Ser. **177**, 388 (2008)
12. C. Theiler, I. Furno, P. Ricci, A. Fasoli, B. Labit, S. Muller, G. Plyushchev, Phys. Rev. Lett. **103**, 065001 (2009)
13. R. Barni, C. Riccardi Plas. Phys. Control. Fusion **51**, 085010 (2009)
14. R. Barni, S. Caldirola, L. Fattorini, C. Riccardi, Phys. of Plas. **24**, 032306 (2017)
15. I. Biganzoli, R. Barni, C. Riccardi, A. Gurioli, R.A. Pertile, Plasma Sources Sci. Technol. **22**, 025009 (2013)
16. S.H. Lee, J. Kim, J.H. Lee, W.H. Choe, Current. Appl. Phys. **10**, 893 (2010)
17. U. Fantz, D. Wunderlich, Atomic Nuclear Data Table **92**, 853 (2004)
18. J.M. Williamson, C.A. DeJoseph Jr., J. Appl. Phys. **93**, 1893 (2003)